Soft Matter

PAPER

View Article Online
View Journal | View Issue

Cite this: *Soft Matter*, 2021, **17**, 2081

Elliptic percolation model for predicting the electrical conductivity of graphene–polymer composites†

Asghar Aryanfar, *[ab] Sajed Medlej,[a] Ali Tarhini[a] and Ali R. Tehrani B[ac]

Received 1st November 2020,
Accepted 21st December 2020

DOI: 10.1039/d0sm01950j

rsc.li/soft-matter-journal

Graphene-based polymers exhibit a conductive microstructure formed by aggregates in a matrix which drastically enhances their transmitting properties. We develop a new numerical framework for predicting the electrical conductivity based on continuum percolation theory in a two dimensional stochastically-generated medium. We analyze the role of the flake shape and its aspect ratio and consequently predict the onset of percolation based on the particle density and the domain scale. Simultaneously, we have performed experiments and have achieved very high electrical conductivity for such composites compared to other film fabrication techniques, which have verified the results of computing the homogenized electrical conductivity. As well, the proximity to and a comparison with other analytical models and other experimental techniques are presented. The numerical model can predict the composite transmitting conductivity in a larger range of particle geometry. Such quantification is exceedingly useful for effective utilization and optimization of graphene filler densities and their spatial distribution during manufacturing.

1 Introduction

Over the last decade, researchers have incorporated graphene-based fillers to improve the electrical conductivity of various polymers.[1–4] The typical electrical conductivity of polymers falls in the range of 10^{-14} to 10^{-17} S cm^{-1}.[5] The significance of particulate graphene is its large aspect ratio.[6] Recently, the solution mixing followed by compression molding method has been utilized to prepare poly-vinylidene fluoride (PVDF) encompassing graphite nanoplatelets (GNPs), where the respective electrical conductivity of the composite has increased from 1.48×10^{-12} S m^{-1} for pure PVDF to 0.032 S m^{-1} for the PVDF composite with 4 wt% of GNP.[7] Additionally, the thermal compression method has improved the electrical conductivity of such composites to ~30 S m^{-1} *via* inclusion of 25 vol% GNFs (graphene nanoflakes).[8] Moreover, the fabrication of self-aligned rLGO/PVDF–HFP (reduced large-area graphene oxide/poly-vinylidene fluoride-*co*-hexafluoropropylene) composite films through a simple solution casting followed by low temperature chemical reduction process achieved an electrical conductivity of ~3000 S m^{-1} for 27.2 wt% of rLGO.[9] Recently, the solution mixing and molding process has led to an ultra-high conductivity value of ~4445 S m^{-1} for a 20 wt% of pure graphene flakes in PVDF–HFP composite.[10]

Percolation theory in fractal media is a conventional approach in modeling the transport properties of composite media,[11–13] where their structure mimics a truncated fractal domain[14] and their physical properties, including the electrical conductivity σ, follow the power law:

$$\sigma \sim (p - p_c)^t$$

where p is the volume fraction of the conductive filler, p_c is the threshold volume fraction for percolation through the entire domain, and t is a dynamic conductivity exponent that depends on the shape and distribution of the fillers.[15] The irregularity of the exponent demonstrates the disorderly behavior in conducting–insulating composites[16] when approaching the percolation threshold from above as the medium becomes highly anisotropic with highly tortuous conducting pathways.[17] Hence, the electrical conductivity is considerably affected by the degree of integration of fillers, which was conveniently obtained with carbon nanotubes at significantly low filling percentages.[18] Guided by this intuition the electrical performance of composites such as polymer–graphene was improved through varying the structural properties, production methods, and post-production routines.[6]

[a] *American University of Beirut, Riad El-Solh 1107, Lebanon. E-mail: aryanfar@caltech.edu*
[b] *Bahçesehir University, 4 Çırağan Cad, Besiktas, Istanbul 34353, Turkey*
[c] *Aalto University, Chemical Engineering, Espoo 02150, Finland*

† Electronic supplementary information (ESI) available. See DOI: 10.1039/d0sm01950j

General effective media (GEM) theory likewise gave approximate formulations to predict the electrical conductivity of composite media[19–21] that are still employed for conductive percolation systems with significant accuracy.[22,23] In these models, the electrical conductivity of a composite of two materials is correlated with the conductivity of both materials, the critical volume fraction, and a power exponent that represents the fractal dimension, conductor–insulator transition point, or the effective demagnetization coefficient of the grain structure.

On the other hand, the electrical conductivity power law was verified by Finite Volume Methods (FVM) and Monte Carlo simulations that calculated the electrical conductivity of PVDF/graphene and other conducting–insulating composites.[24,25] The results of these numerical models displayed the dependence of the electrical conductivity on the spatial distribution of filler particles inside the composite as they could vary from stochastic to Gaussian. Moreover, the percolation threshold for conductance decreases with the particle aspect ratio.

The presented work is structured as follows. In Section 3 we present the technique of producing the highly connected graphene–polymer composite films and the adopted procedure for measuring the electrical conductivity across the films. Section 2 demonstrates the formulation of the novel numerical percolation model and the generation of the stochastic particle domains. Then, in Section 4, our results are compared with documented results and the suggested model is validated and compared with previously proposed analytical models of composite material conductivity. Section 5 concludes the article with a summary of the major findings and suggestions for future work.

2 Modeling

We present a new framework to estimate the effective electrical conductivity of polymer–graphene composites using a percolation model with stochastically distributed particles based on their geometry and the domain scale. The process is divided into four major routines as shown in Fig. 1 and explained in detail below:

2.1 Initialization

The generated graphene particles are considered elliptical in shape with varying aspect ratios deduced from Fig. 3a. The particles have semi-major and semi-minor axes $\{a,b\}$ with center coordinates of (x_i,y_i) and respective orientation θ_i where N is their multiplicity. The geometric dimensions of the ellipses are generated proportionally to the number density of particles in the normalized domain such that $\{a,b\} \sim 1/N$ with N ellipses dispersed per iteration, and hence we define the aspect ratio as $r := \frac{b}{a}$ varying within $r \in \{0.02, 0.08\}$ to identify the parameters that properly represent the graphene–polymer medium.

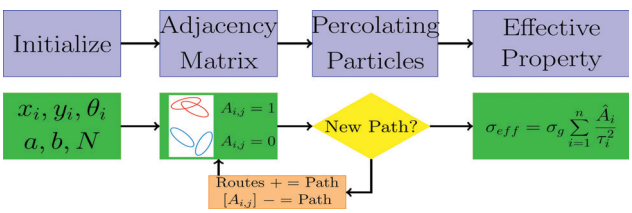

Fig. 1 Pseudo-flowchart of the numerical procedure and signature steps in each sub-routine for extracting the homogenized conductivity of graphene flakes mixed in a polymer matrix.

2.2 Adjacency evaluation

The connection of the percolating clusters is defined by the adjacency matrix $A_{i,j}$. The equation of an individual ellipse with semi-major and semi-minor axes of a and b, centered at position (x_i,y_i), and rotated by angle θ_i, is given by:

$$\frac{1}{a^2}((x-x_i)\cos\theta_i + (y-y_i)\sin\theta_i)^2 + \frac{1}{b^2}((x-x_i)\sin\theta_i - (y-y_i)\cos\theta_i)^2 = 1 \quad (1)$$

There is a simple model to check whether two ellipses that are described by eqn (1) intersect which illustrates the use of the Vieillard–Baron contact function Ψ [26] and the coefficients f_1 and f_2 used frequently for elliptic percolation as:[27–29]

$$\begin{cases} \Psi = 4(f_1{}^2 - 3f_2)(f_2{}^2 - 3f_1) - (9 - f_1 f_2)^2 \\ f_\beta = 3 + A - B - C \\ A = \left(\frac{a}{b} - \frac{b}{a}\right)^2 \sin^2(\theta_2 - \theta_1) \\ B = \frac{1}{a^2}((x_2 - x_1)\cos\theta_\beta + (y_2 - y_1)\sin\theta_\beta)^2 \\ C = \frac{1}{b^2}((y_2 - y_1)\cos\theta_\beta - (x_2 - x_1)\sin\theta_\beta) \end{cases}$$

where β = 1, 2 are the subscripts denoting the two ellipses. f_1 and f_2 are the coefficients in the cubic polynomial of eigenvalues derived by setting the determinant of the pencil of conics of the intersection points between the two ellipses to zero, and Ψ is the discriminant of this determinant.[26] The connection criterion is thus extracted from the sign of the discriminant and determinant coefficients as follows:[26]

$$\begin{cases} \Psi < 0 \\ \text{or} \qquad \rightarrow \text{Intersect} \\ \{\Psi, f_1, f_2\} > 0 \end{cases}$$

Subsequently, the adjacency matrix $A_{ij}(N^2 \times N^2)$ is created for percolation computations through the entire medium, which is then utilized to investigate the existence of percolation passages.

2.3 Percolation pathways

Continuum percolation is performed at each iteration depending on the available connected ellipses from the edges of the medium, and the shortest connecting pathways are selected. Consequently, they are added to the list of percolation pathways, and new unique and optimal pathways are re-scanned iteratively until none are found. For optimal path detection, Dijkstra's algorithm is utilized,[30] which is not only used for

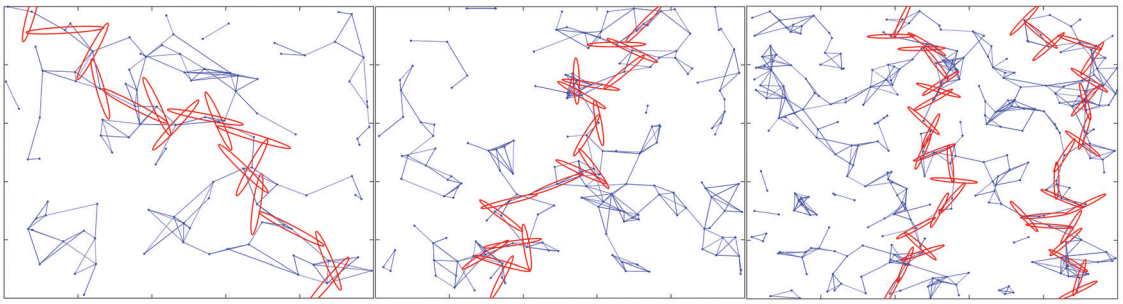

(a) Blue: Partial percolation clusters. Red: end-to-end percolation pathways.

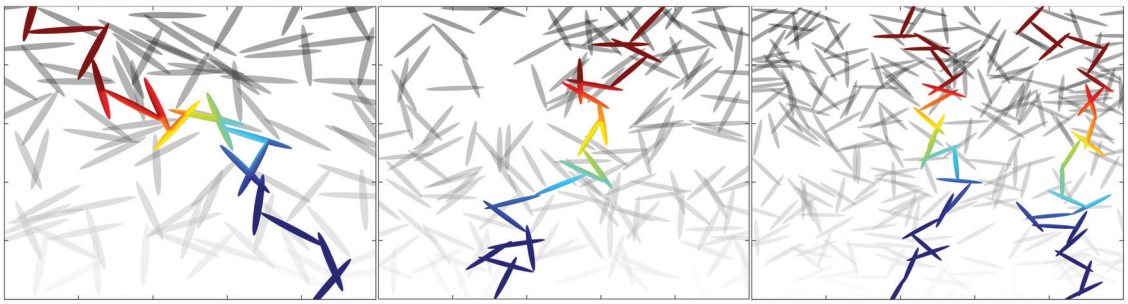

(b) Respective color-indexed particles representing their proximity to the boundary.

Fig. 2 Top: Pathways of continuum elliptic percolation with a filler aspect ratio of r = 0.05 and a domain scale of L = {225, 400, 625} for the left, center and right images, respectively. Bottom: The color-indexed pathways, representing their proximity to the domain boundary.

elliptical percolation,[31,32] but also proved beneficial in cases including, but not limited to, path-planning,[33–35] chemical particle distributions,[36] combustion kinetics,[37] and anatomical therapeutic drug detection.[38]

The Dijkstra algorithm depends on contacting ellipses and assigns costs for paths as the normal distance between the centers of the ellipses in comprising the path. For this purpose, the adjacency matrix A_{ij} computed above is coupled with the positions of the particles (x_i, y_i) to compute the normal distances and generate the cost matrix C_{ij}. These costs are represented by the blue segments in Fig. 2a, and show the background graph of connections. The algorithm starts from a set of ellipses and finds local minimum cost connections to reach the final destination. The search for the starting and ending particles is limited to those within a distance of a from any of the boundaries. Whenever a new shorter path is found through a different, but not necessarily unique, set of contact ellipses, the previous longer path is replaced by the new optimized path. Fig. 2b shows for a randomly generated set of ellipses the unique and most optimal percolation paths.

2.4 Effective conductivity

An intermediate parameter is the cluster size of partial connection to only one edge ($\hat{A}_{\text{part}}$), which is normalized and computed using the burning algorithm.[28] The forward percolation starts from one side of the domain, and moves sequentially through the connected particles *via* 1st-order neighbors until no further progress is made.

The additional computed parameters include the normalized area of pathways $\hat{A}_i$ and their respective tortuosity τ_i. The computation of overlapped areas can be performed *via* the Polyshape MATLAB toolkit. The merged non-uniform shape is illustrated by comparing the intersections of red particles in Fig. 2a and the joined color-coded pathways in Fig. 2b.

The individual tortuosity τ_i is calculated as:

$$\tau_i = \frac{l_i}{d_i} \tag{2}$$

where l_i and d_i are the total length and shortest distance between the path edges. As such, the homogenized electrical conductivity σ_{eff}, the homogenized effective electrical conductivity of the medium, can be calculated noting the porosity $\hat{A}_{\text{tot}}$ and individual tortuosity of pathways τ_i as follows:[39,40]

$$\sigma_{\text{eff}} = \sigma_{\text{g}} \frac{\hat{A}_{\text{tot}}}{\tau^2} = \sigma_{\text{g}} \sum_{i=1}^{n} \frac{\hat{A}_i}{\tau_i^2} \tag{3}$$

where σ_{g} is the electrical conductivity of graphene, and $\hat{A}_i$ is the normalized area of the optimal percolation pathways at each realization of the domain. Moreover, the estimation of the saturated area $\hat{A}_{\text{tot}}$ is stochastically computed *via* the following:

$$\hat{A}_{\text{tot}} = 1 - \text{e}^{-N\frac{A_{\text{e}}}{A_{\text{d}}}} \tag{4}$$

where A_{d} is the area of the simulated domain, and $A_{\text{e}} = \pi ab = \pi r a^2$ is the area of a single ellipse. $\hat{A}_{\text{tot}}$ is the total filling area of the particles in the domain representing the graphene phase, which is calculated based on the excluded volume principle.[41]

3 Experimental

Graphene flakes with 98.5% purity from Graphene 3D Lab Inc. (US) and *N*,*N*-dimethylformamide (DMF) and the PVDF–HFP copolymer at 25 °C from Sigma-Aldrich (Germany) were used. The composite samples were molded in a heat resistant cubical silicone mold with multiple cavities from Silikomart (Italy). The flakes were approximated with an elliptical shape of a longitudinal length of $l_p \approx 7$ μm and thickness $t_p \simeq 1.1$ nm given by the manufacturer. As a result, we have very large flake aspect ratios in the bilateral direction $l_p/t_p \sim 10^3$, which favors domination of the effective transport along the plane of the flakes. The particle length l_p is verified through image processing of sample sections of the produced composite films as shown in Fig. 3a.

Several samples of the graphene–polymer composite films stated in Fig. 3b were produced with different graphene weight content, which was calculated using the simple mixing rule:

$$\rho_C = (1 - W) \times \rho_P + W \times \rho_G$$

where ρ_C is the density of the composite, $\rho_P \sim 1.8$ g mL^{-1} is the density of the polymer, $\rho_G \sim 2.2$ g cm^{-3} is the density of graphene, and W is the weight percentage of graphene. The process of producing the films comprised several ordered steps as follows (Table 1):

1. Mix the graphene dispersion with the polymer mixture according to the volume sets in Fig. 3b.

2. Mold the mixed solution to form polymeric composite films with various graphene wt%.

3. Evaporate the solvent (DMF) from the solution. DMF was used to dissolve PVDF–HFP copolymer pellets. It was also used to dissolve graphene powder creating a graphene dispersion, where the dispersion was then bath sonicated for 30 min at 35 °C.

4. Heat to a temperature of ~70 °C and then stir for 10–15 min using a magnetic stirrer (500–1000 rpm), and after that pour the solution into a cavity in the silicone mold. Finally, place the mold inside an electric oven for 24 h at 90 °C after making sure that the solvent (DMF) was evaporated entirely from the mixture of each sample.

The surface morphology for every sample was inspected using a MIRA 3 LMU, a scanning electron microscope from Tescan Inc., at an accelerating voltage of 20 V as shown in Fig. 4. The graphene–polymer binarization (black and white) was done *via* thresholding using Otsu's method[42] where the values below the threshold represent the composite polymer and graphene flakes are in red otherwise. The thickness of each film was measured using a gauge from MP1 Brunswick Instrument with 2 μm resolution. The electrical conductivity for each film was measured using a four-point probe system from Ossila (UK). For the in-plane electrical conductivity, the change in the voltage across the inner two probes is measured when current is passed between the outer two probes. The electrical conductivity (σ) was calculated using this equation:

$$\sigma = \frac{\ln(2)}{\pi} \frac{I}{d \cdot \Delta V}$$

where d is the composite film thickness, I is the measured electrical current across the sample, and ΔV is the measured voltage difference. Each film was measured 25 times, and the average value was reported for each film. For each measurement, composite films with the following dimensions (length: 30 mm; width: 15 mm; and thickness: 0.2–0.5 mm) were used.

4 Results and discussion

The proper choice of parameters for predicting the electrical conductivity of graphene–polymer composites is a complex process. We have developed a systematic procedure for properly choosing the parameters, utilizing the intrinsic properties of the percolating media of such cluster features and thresholds,[43,44] as well as identifying the role of the particle aspect ratio.[45–48] The trend of the tortuosity in Fig. 5a shows an asymptotic decrease

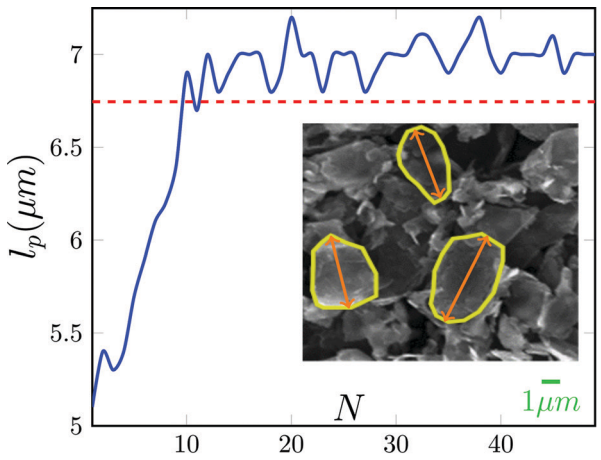

(a) Distribution of flake size l_p.

V_g (mL)	V_p (mL)	W (%)
1	25	0.99
6	25	5.6
11	25	9.9
15	15	20
20	15	25
20	10	33
20	5	50

(b) Composite recipes.

Fig. 3 Experimental procedure. Left: Statistical tracking of particle size for a sample cross section of the graphene–polymer film. Right: The selected volumes for the included graphene, where the weight ratio is calculated from the densities of graphene ρ_g [5 g L^{-1}] and the polymer ρ_p [20 g L^{-1}], respectively.

Table 1 Best attempts to enhance the electrical conductivity of polymers using graphene with weight ratios $\hat{w}_g$ using different fabrication techniques. The achieved electrical conductivity for composites with different graphene wt% is presented

Composition of films	Preparation method	$\hat{w}_g$ (wt%)	$\sigma_{Exp.}$ (S m^{-1})
GNP solution in PVDF[7]	Solution mixing, casting and hot pressing	4	0.031
Graphene oxide (GO) in PVDF[49]	Solution mixing, GO reduction using solar radiation	7	10
Graphene flakes incorporated in PVDF–HFP[10]	Vigorous solution mixing, molding	20	4445
rLGO in PVDF–HFP[50]	Solution mixing, casting, chemical reduction	27.2	3000
Functionalized graphene sheets with nanodiamond fillers (FGS/ND) with PVDF[51]	Ultrasonic dispersion, hot pressing	45	7.1×10^{-5}
GNF solution in PVDF[8]	Melt compression of graphene with PVDF in an L-shaped tube	25 vol%	30

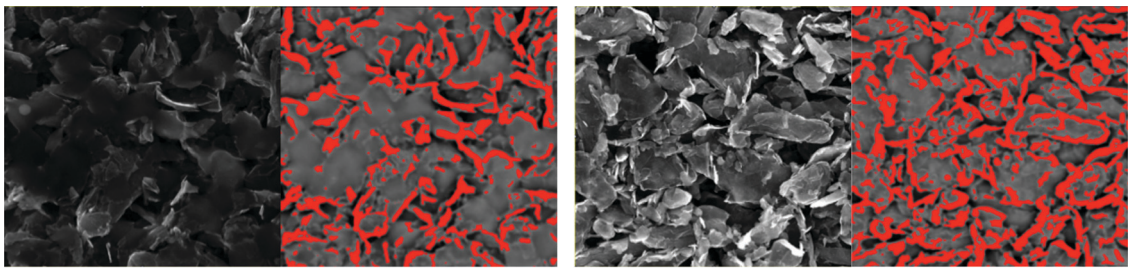

(a) $W \approx 6\%$ (b) $W = 20\%$

Fig. 4 Grayscale: SEM images of the graphene flakes. Color: the binarized image distinguishing the filler from the matrix, for two weight percentages W of graphene.

towards its lower bound of $\tau = 1$. Therefore, the higher multiplicity of the graphene particles provides more straight pathways for percolation. The percolation threshold is the smallest for the lowest aspect ratio, representing the best possibility of overlapping for elongated particles for connection. On the contrary, the low aspect ratio particles ($r \to 1$) tend to accumulate more with lower feasibility of overlapping. Note that the saturation of the total area correlates non-linearly with the particle density in the domain *via* eqn (4).[27,29,48] Thus, more graphene particle saturation provides higher conductivity, albeit less effectively.

As well, in Fig. 5b the saturation in the partial percolation pathways shows direct correlation with the original porosity $\hat{A}_{tot}$. The largest percolation cluster belongs to the elongated particles (*i.e.* low aspect ratio) due to higher probability of overlapping. As well, the early saturation of the medium in this figure shows the effectiveness of the partial clusters, consistent with Fig. 4. Although partial pathways are frequent, they typically rarely complete to the other side, especially beyond the percolation threshold.

It is also critical to determine the surface area ratio of graphene to the polymer from the SEM images in Fig. 4. The simulated effective

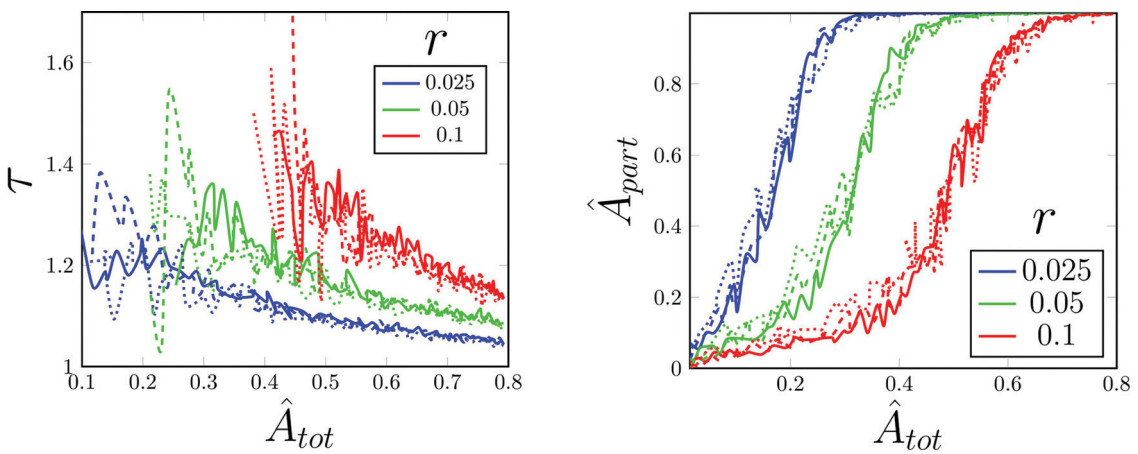

(a) Tortuosity of percolating pathways. (b) Area of percolating clusters from the domain boundary.

Fig. 5 Computed tortuosity (left) and the fractional area of percolating clusters from the boundary based on the domain scale (dotted $L = 225$, dashed $L = 400$, solid $L = 600$).

percolation pathway area for various aspect ratios ($\hat{A}_{\text{eff}} = \sum \hat{A}_i$) *via* flowchart Fig. 1 and theoretical calculations of the effective areas were in agreement, and they lie in the region of particles with aspect ratios $r \in [0.02, 0.05]$. Although the particle longitudinal dimension was measured to be $l_p \sim 7$ μm with an approximate aspect ratio of ≈0.5 as shown in Fig. 3a, the behavior of the particles, particularly at higher scales, shows a strip-like agglomeration of particles that is better represented by high aspect ratio ellipses of lower density. This behavior can be attributed to the fabrication process where graphene flakes aggregate to form thin interfaces adjacent to polyhedral polymer particles[52,53] as seen in the SEM images (Fig. 4). Additionally, the size and aspect ratio of graphene particles may change during the preparation of the composites due to high speed mechanical mixing of the graphene dispersions. As a result, the effective flake size of the graphene flakes may be much smaller than seen in Fig. 3a.

Therefore, we proceeded with calculating the total electrical conductivity of the medium according to eqn (3) for a set of aspect ratios of $r = \{0.025, 0.05, 0.1\}$ for the proper applicability of continuum percolation theory to the experimental samples. It is needless to mention that the performance of the simulations in 2D and the experiments in 3D is another source of deviation. The 3D experiments lead to less overlapping of the particles, which correlates with the 2D planar simulations of higher aspect ratio.

Fig. 6a shows that the normalized percolation cluster density $\hat{\rho}(L)$ reduces with the scale of the medium L *versus* various particle aspect ratios. This is approximated by the power law:

$$\hat{\rho}(L) \sim L^{D-d}$$

where D is the fractal dimension of the medium and $d = 2$ for a 2D domain.[54] As well, the extracted power coefficient shows faster decline in the density for the highest individual aspect ratio (*i.e.* circle-like) since the connectivity is more hampered on larger scales. This is a result of the high number clustering and low connectedness, which creates larger voids. *Vice versa*, the density of particles with lower individual aspect ratio (*i.e.* smear-like) declines less rapidly with scale since they maintain more connected clusters stretching through the domain.

Fig. 6b is a plot of the effective electrical conductivity of the graphene–polymer composite as a function of the total filling area of particles. The experimental results (red crosses) and the elliptic simulation values (blue curves) are compared against the experimental values in the literature[8,9,55] and the theoretical understanding.[56–58] The experimental values are lower than the computational results for the most part, emphasizing the higher possibility of intersection in 2D (simulations) relative to 3D (experiments), given the same density of particles.

The SEM images in Fig. 4 show that the larger particles of coagulated graphene are connected to smaller pigments that vary in aspect ratio and percolating area.

The models for predicting the conductivity of composite materials are presented in Fig. 5. The first model is the classical percolation power law approximation[59,60] suggested in ref. 58:

$$\sigma_{\text{eff}} = \sigma_g \left(\frac{\hat{A} - \hat{A}_c}{1 - \hat{A}_c} \right)^t; \quad \hat{A} > \hat{A}_c \tag{5}$$

where $\hat{A}_c$ is the normalized area ratio at the percolation threshold, and t is a power constant given in Table 2. Although this model accurately predicts the percolation threshold and the conductivity beyond it, it possesses an asymptotic limit at the percolation threshold. For $\hat{A} < \hat{A}_c$, the model cannot explain the conductivity of the polymer at extemely low graphene contents, whereas for $\hat{A} > \hat{A}_c$ the model is driven by particle aggregates where σ_{pm}, the electrical conductivity of the polymer matrix, becomes relatively infinitesimally small.[59]

Another semi-analytical model describes the limiting transition between the non-conducting and conducting phases of the mixture, established based on the Fermi–Dirac distribution:[56]

$$\log(\sigma_{\text{eff}}) = \log(\sigma_g) + \frac{\log(\sigma_{pm}/\sigma_g)}{1 - e^{b(\hat{A} - \hat{A}_c)}} \tag{6}$$

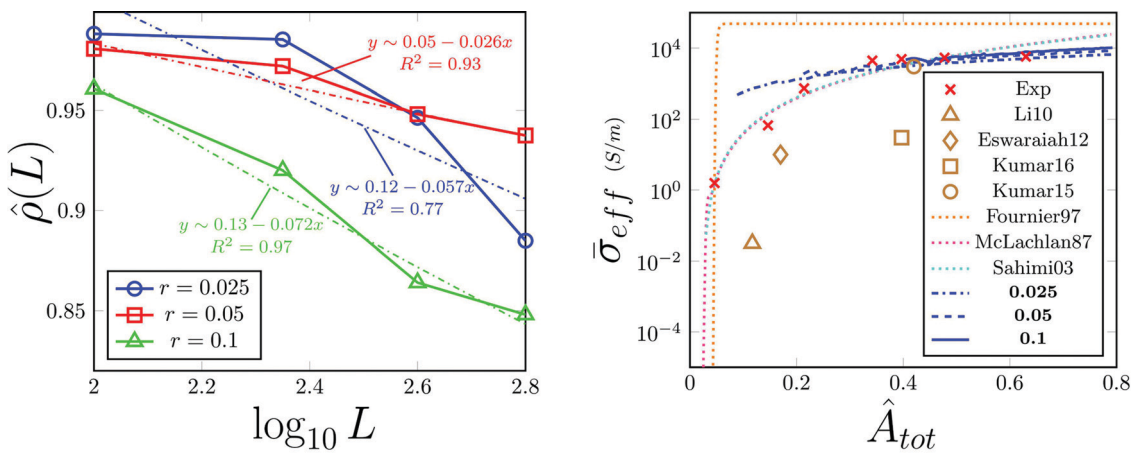

(a) Cluster density. (b) The conductivity comparison.

Fig. 6 Left: The in-plane percolation cluster density *versus* the normalized domain length scale with the variation in the particle aspect ratio. Right: The conductivity comparison of simulations/experiment/literature data (×: experimental values; Δ, □, ○, ◊: literature values; …: theoretical models; blue: elliptic simulations with variant aspect ratio).

Table 2 Constant parameters for electrical conductivity estimation models

Model	$\hat{A}_c$	t	b	R^2
Sahimi 03[12]	0.023	2.76	—	0.9635
Fournier 97[56]	0.0435	—	448	0.9405
Mclachlan 87[57]	0.0205	2.85	—	0.9634

where b is a fitting parameter that controls the rate of the conductivity transition from the insulating to the conducting phase through the percolation threshold. Although this model has a continuous domain across the percolation threshold, its predictions diverge away from the experimental results. The model appears to be rigid in its description of the transition between the insulating phase ($\hat{A} < \hat{A}_c$) and the conductive phase ($\hat{A} > \hat{A}_c$) where the transition becomes very steep at the percolation threshold.

The final model illustrated in Fig. 6a corrects the general effective media theory (GEM) with percolation principles to properly estimate the binary media properties of various particle dispersion geometries,[57] which is described as:[61]

$$\begin{cases} \sigma_{\text{eff}} = \sigma_{\text{pm}}\left[\Omega + \sqrt{\Omega^2 + \left(\dfrac{\hat{A}_c}{1-\hat{A}_c}\right)\left(\dfrac{\sigma_g}{\sigma_{\text{pm}}}\right)^{1/t}}\right]^t \\ \Omega = \dfrac{1}{2(1-\hat{A}_c)}\left[1 - \hat{A}_c - \hat{A} + (\hat{A} - \hat{A}_c)\left(\dfrac{\sigma_g}{\sigma_{\text{pm}}}\right)^{1/t}\right] \end{cases} \quad (7)$$

The models in eqn (7) and (5) have closely predicted the percolation limit and transport percolation exponent, where McLachlan suggests a smoother transition between the low and high conductivity phases similar to the results produced by our numerical model.

5 Conclusion

To produce graphene–polymer composite films with exceptionally high electrical conductivity, we incorporated 98.5% pure graphene flakes into PVDF-HEP through rapid vortex mixing at elevated temperatures, which led to the formation of highly connected graphene clusters. Subsequently, we developed a novel percolation-based numerical model to predict and analyze such enhancement by utilizing stochastic continuum realizations of dispersed elliptic particles in 2D planes. The optimal percolation pathways obtained through Dijkstra's algorithm become dominant predictors of the electrical conductivity of the homogenized conductor–insulator medium above the percolation threshold.

The adopted experimental procedure has surpassed the electrical conductivity for previously-reported lower dispersed graphene density. The model correlates well with the experimental results and is in agreement with the theoretical understandings. The low scale-sensitivity of the tortuosity and partially-formed clusters to the original particle density and aspect ratio shows the applicability of the results independent of the magnitude. The simulated particles with low aspect ratio showed better inter-connectedness and enhanced conductivity, especially at higher scales.

Overall, the presented fabrication technique showed its advantage over reported methodologies and can be easily used to produce highly conductive composite films. On the other hand, the suggested percolation-based numerical model showed its compatibility in tackling composite media properties, and future developments are directed towards encompassing the variation and multiplicity in the particle shape and aspect ratio, as well as expanding the model prior to the percolation threshold and analyzing its sensitivity in its neighborhood.

Author contributions

Asghar Aryanfar: Conceptualization, Validation, Formal Analysis, Investigation, Data Curation, Writing Original/Final Drafts, Visualization, Funding Acquisition. Sajed Medlej: Programming, Methodology, Writing – Review/Editing, Ali Tarhini: Experimentation, Writing. Ali Tehrani, PhD: Supervision, Funding Acquisition.

Conflicts of interest

The authors declare no competing financial interest regarding this publication.

Acknowledgements

The authors would like to thank and recognize the PhD fellowship for graduate students Sajed Medlej and Ali Tarhini from MSFEA Engineering faculty at American University of Beirut.

References

1 L. C. Costa and F. Henry, Dc electrical conductivity of carbon black polymer composites at low temperatures, *J. Non-Cryst. Solids*, 2011, **357**(7), 1741–1744.
2 Jiaxi Guo, Nicholas Briggs, Steven Crossley and Brian P Grady, A new finding for carbon nanotubes in polymer blends: Reduction of nanotube breakage during melt mixing, *J. Thermoplast. Compos. Mater.*, 2018, **31**(1), 110–118.
3 Z.-L. Hou, W.-L. Song, P. Wang, M. J. Meziani, C. Y. Kong, A. Anderson, H. Maimaiti, G. E. LeCroy, H. Qian and Y.-P. Sun, Flexible graphene–graphene composites of superior thermal and electrical transport properties, *ACS Appl. Mater. Interfaces*, 2014, **6**(17), 15026–15032.
4 Y. Huang, S. Kormakov, X. He, X. Gao, X. Zheng, Y. Liu, J. Sun and D. Wu, Conductive polymer composites from renewable resources: an overview of preparation, properties, and applications, *Polymers*, 2019, **11**(2), 187.
5 M. L. Clingerman, J. A. King, K. H. Schulz and J. D. Meyers, Evaluation of electrical conductivity models for conductive polymer composites, *J. Appl. Polym. Sci.*, 2002, **83**(6), 1341–1356.

6 A. J. Marsden, D. G. Papageorgiou, C. Vallés, A. Liscio, V. Palermo, M. A. Bissett, R. J. Young and I. A. Kinloch, Electrical percolation in graphene–polymer composites, *2D Mater.*, 2018, **5**(3), 032003.
7 Y. C. Li, S. C. Tjong and R. K. Y. Li, Electrical conductivity and dielectric response of poly(vinylidene fluoride)-graphite nanoplatelet composites, *Synth. Met.*, 2010, **160**(17–18), 1912–1919.
8 H. Jung, S. Yu, N.-S. Bae, S. M. Cho, R. H. Kim, S. H. Cho, I. Hwang, B. Jeong, J. S. Ryu and J. Hwang, *et al.*, High through-plane thermal conduction of graphene nanoflake filled polymer composites melt-processed in an l-shape kinked tube, *ACS Appl. Mater. Interfaces*, 2015, **7**(28), 15256–15262.
9 P. Kumar, S. Yu, F. Shahzad, S. M. Hong, Y.-H. Kim and C. M. Koo, Ultrahigh electrically and thermally conductive self-aligned graphene/polymer composites using large-area reduced graphene oxides, *Carbon*, 2016, **101**, 120–128.
10 A. A. Tarhini and A. R. Tehrani-Bagha, Graphene-based polymer composite films with enhanced mechanical properties and ultra-high in-plane thermal conductivity, *Compos. Sci. Technol.*, 2019, **184**, 107797.
11 V. K. S. Shante and S. Kirkpatrick, An introduction to percolation theory, *Adv. Phys.*, 1971, **20**(85), 325–357.
12 M. Sahimi, *Heterogeneous materials I: linear transport and optical properties*, Springer Science & Business Media, 2003, vol. 22.
13 A. Aharony and D. Stauffer, *Introduction to percolation theory*, Taylor & Francis, 2003.
14 A. G. Hunt, Continuum percolation theory for transport properties in porous media, *Philos. Mag.*, 2005, **85**(29), 3409–3434.
15 M. A. Dubson and J. C. Garland, Measurement of the conductivity exponent in two-dimensional percolating networks: square lattice versus random-void continuum, *Phys. Rev. B: Condens. Matter Mater. Phys.*, 1985, **32**(11), 7621.
16 S. Mertens and C. Moore, Continuum percolation thresholds in two dimensions, *Phys. Rev. E: Stat., Nonlinear, Soft Matter Phys.*, 2012, **86**(6), 061109.
17 A. Celzard and J. F. Marêché, Non-universal conductivity critical exponents in anisotropic percolating media: a new interpretation, *Phys. A*, 2003, **317**(3–4), 305–312.
18 M. Foygel, R. D. Morris, D. Anez, S. French and V. L. Sobolev, Theoretical and computational studies of carbon nanotube composites and suspensions: electrical and thermal conductivity, *Phys. Rev. B: Condens. Matter Mater. Phys.*, 2005, **71**(10), 104201.
19 D. S. McLachlan, Equations for the conductivity of macroscopic mixtures, *J. Phys. C: Solid State Phys.*, 1986, **19**(9), 1339.
20 D. S. McLachlan, Measurement and analysis of a model dual-conductivity medium using a generalised effective-medium theory, *J. Phys. C: Solid State Phys.*, 1988, **21**(8), 1521.
21 D. S. McLachlan, Equation for the conductivity of metal–insulator mixtures, *J. Phys. C: Solid State Phys.*, 1985, **18**(9), 1891.
22 W. Xu, Z. Zhu and D. Zhang, Continuum percolation-based tortuosity and thermal conductivity of soft superball systems: shape dependence from octahedra via spheres to cubes, *Soft Matter*, 2018, **14**(43), 8684–8691.
23 Y. Chen and C. A. Schuh, Diffusion on grain boundary networks: Percolation theory and effective medium approximations, *Acta Mater.*, 2006, **54**(18), 4709–4720.
24 A. Manta, M. Gresil and C. Soutis, Predictive model of graphene based polymer nanocomposites: electrical performance, *Appl. Compos. Mater.*, 2017, **24**(2), 281–300.
25 A. B. Oskouyi, U. Sundararaj and P. Mertiny, Tunneling conductivity and piezoresistivity of composites containing randomly dispersed conductive nano-platelets, *Materials*, 2014, **7**(4), 2501–2521.
26 J. Vieillard-Baron, Phase transitions of the classical hard-ellipse system, *J. Chem. Phys.*, 1972, **56**(10), 4729–4744.
27 W. Xia and M. F. Thorpe, Percolation properties of random ellipses, *Phys. Rev. A: At., Mol., Opt. Phys.*, 1988, **38**(5), 2650.
28 Y.-B. Yi and A. M. Sastry, Analytical approximation of the two-dimensional percolation threshold for fields of overlapping ellipses, *Phys. Rev. E: Stat., Nonlinear, Soft Matter Phys.*, 2002, **66**(6), 066130.
29 J. Li and M. Östling, Precise percolation thresholds of two-dimensional random systems comprising overlapping ellipses, *Phys. A*, 2016, **462**, 940–950.
30 E. W. Dijkstra, *et al.*, A note on two problems in connexion with graphs, *Numer. Math.*, 1959, **1**(1), 269–271.
31 Z. Pan, D. Wang, R. Ma and A. Chen, A study on itz percolation threshold in mortar with ellipsoidal aggregate particles, *Comput. Concr.*, 2018, **22**(6), 551–561.
32 A. Plyushch, P. Lamberti, G. Spinelli, J. Macutkevič and P. Kuzhir, Numerical simulation of the percolation threshold in non-overlapping ellipsoid composites: toward bottom-up approach for carbon based electromagnetic components realization, *Appl. Sci.*, 2018, **8**(6), 882.
33 G. Qing, Z. Zheng and X. Yue, Path-planning of automated guided vehicle based on improved dijkstra algorithm, in *2017 29th Chinese control and decision conference (CCDC)*, IEEE, 2017, pp. 7138–7143.
34 H. Il Kang, B. Lee and K. Kim, Path planning algorithm using the particle swarm optimization and the improved dijkstra algorithm, in *2008 IEEE Pacific-Asia Workshop on Computational Intelligence and Industrial Application*, IEEE, 2008, vol. 2, pp. 1002–1004.
35 H. Wang, Y. Yu and Q. Yuan, Application of dijkstra algorithm in robot path-planning, in *2011 second international conference on mechanic automation and control engineering*, IEEE, 2011, pp. 1067–1069.
36 A. Katunin, Generalized chemical distance distribution in all-sided critical percolation clusters, in *AIP Conf. Proc.*, AIP Publishing LLC, 2016, vol. 1790, p. 150002.
37 Y. Chen and J.-Y. Chen, Towards improved automatic chemical kinetic model reduction regarding ignition delays and flame speeds, *Combust. Flame*, 2018, **190**, 293–301.
38 L. Chen, T. Liu and X. Zhao, Inferring anatomical therapeutic chemical (atc) class of drugs using shortest path and

random walk with restart algorithms, *Biochim. Biophys. Acta, Mol. Basis Dis.*, 2018, **1864**(6), 2228–2240.

39 L. De Backer and G. Baron, Effective diffusivity and tortuosity in a porous glass immobilization matrix, *Appl. Microbiol. Biotechnol.*, 1993, **39**(3), 281–284.

40 L. Shen and Z. Chen, Critical review of the impact of tortuosity on diffusion, *Chem. Eng. Sci.*, 2007, **62**(14), 3748–3755.

41 K. Meeks, M. L. Pantoya, M. Green and J. Berg, Extending the excluded volume for percolation threshold estimates in polydisperse systems: the binary disk system, *Appl. Math. Model.*, 2017, **46**, 116–125.

42 C. Yu, C. Dian-ren, L. Yang and C. Lei, Otsu's thresholding method based on gray level-gradient two-dimensional histogram, in *Proceedings of the 2nd International Asia Conference on Informatics in Control, Automation and Robotics – Volume 3, CAR'10*, IEEE Press, 2010, pp. 282–285.

43 S. Torquato and Y. Jiao, Effect of dimensionality on the percolation threshold of overlapping nonspherical hyperparticles, *Phys. Rev. E: Stat., Nonlinear, Soft Matter Phys.*, 2013, **87**(2), 022111.

44 S. B. Lee and S. Torquato, Measure of clustering in continuum percolation: computer-simulation of the two-point cluster function, *J. Chem. Phys.*, 1989, **91**(2), 1173–1178.

45 Y.-B. Yi and A. M. Sastry, Analytical approximation of the percolation threshold for overlapping ellipsoids of revolution, *Proc. R. Soc. London, Ser. A*, 2004, **460**(2048), 2353–2380.

46 M. Ambrožič, The percolation threshold in systems of permeable ellipses, *Eur. Phys. J.: Appl. Phys.*, 2008, **41**(2), 121–127.

47 E. Pervago, A. Mousatov, E. Kazatchenko and M. Markov, Computation of continuum percolation threshold for pore systems composed of vugs and fractures, *Comput. Geosci.*, 2018, **116**, 53–63.

48 J. Lin and H. Chen, Measurement of continuum percolation properties of two-dimensional particulate systems comprising congruent and binary superellipses, *Powder Technol.*, 2019, **347**, 17–26.

49 V. Eswaraiah, K. Balasubramaniam and S. Ramaprabhu, One-pot synthesis of conducting graphene–polymer composites and their strain sensing application, *Nanoscale*, 2012, **4**(4), 1258–1262.

50 P. Kumar, F. Shahzad, S. Yu, S. M. Hong, Y.-H. Kim and C. M. Koo, Large-area reduced graphene oxide thin film with excellent thermal conductivity and electromagnetic interference shielding effectiveness, *Carbon*, 2015, **94**, 494–500.

51 J. Yu, R. Qian and P. Jiang, Enhanced thermal conductivity for pvdf composites with a hybrid functionalized graphene sheet-nanodiamond filler, *Fibers Polym.*, 2013, **14**(8), 1317–1323.

52 H. Pang, T. Chen, G. Zhang, B. Zeng and Z.-M. Li, An electrically conducting polymer/graphene composite with a very low percolation threshold, *Mater. Lett.*, 2010, **64**(20), 2226–2229.

53 L. Guadagno, M. Raimondo, L. Vertuccio, M. Mauro, G. Guerra, K. Lafdi, B. De Vivo, P. Lamberti, G. Spinelli and V. Tucci, Optimization of graphene-based materials outperforming host epoxy matrices, *RSC Adv.*, 2015, **5**(46), 36969–36978.

54 D. Stauffer and A. Aharony, *Introduction to percolation theory*. CRC Press, 1994.

55 Y. Cao, M. Liang, Z. Liu, Y. Wu, X. Xiong, C. Li, X. Wang, N. Jiang, J. Yu and C.-T. Lin, Enhanced thermal conductivity for poly(vinylidene fluoride) composites with nano-carbon fillers, *RSC Adv.*, 2016, **6**(72), 68357–68362.

56 J. Fournier, G. Boiteux, G. Seytre and G. Marichy, Percolation network of polypyrrole in conducting polymer composites, *Synth. Met.*, 1997, **84**(1–3), 839–840.

57 D. S. McLachlan, An equation for the conductivity of binary mixtures with anisotropic grain structures, *J. Phys. C: Solid State Phys.*, 1987, **20**(7), 865.

58 I. Alig, D. Lellinger, M. Engel, T. Skipa and P. Pötschke, Destruction and formation of a conductive carbon nanotube network in polymer melts: In-line experiments, *Polymer*, 2008, **49**(7), 1902–1909.

59 S. Havlin and A. Bunde, Percolation ii, in *Fractals and disordered systems*, Springer, 1991, pp. 97–150.

60 D. Stauffer and A. Aharony, *Introduction to percolation theory*, Taylor & Francis, London, Washington, DC, vol. 96, 1992.

61 H. Deng, T. Skipa, R. Zhang, D. Lellinger, E. Bilotti, I. Alig and T. Peijs, Effect of melting and crystallization on the conductive network in conductive polymer composites, *Polymer*, 2009, **50**(15), 3747–3754.